IV International Conference on Computational Methods for Coupled Problems in Science and Engineering
COUPLED PROBLEMS 2011
M. Papadrakakis, E. Oñate and B. Schrefler (Eds)

FINITE VOLUME AND FINITE ELEMENT SCHEMES FOR THE EULER EQUATIONS IN CYLINDRICAL AND SPHERICAL COORDINATES

DANTE DE SANTIS*, GIANLUCA GERACI* AND ALBERTO GUARDONE†

*INRIA Bordeaux–Sud-Ouest, èquipe-projet Bacchus
Cours de la Libération, 33405 Talence, France
e-mail: dante.de_santis@inria.fr, gianluca.geraci@inria.fr

†Dipartimento di Ingegneria Aerospaziale
Politecnico di Milano
Via La Masa 34, 20156 Milano, Italy
e-mail: alberto.guardone@polimi.it

Key words: Compressible flows, Cylindrical/Spherical Coordinates, Explosion problem, Finite Element/Volume Methods.

Abstract. A numerical scheme is presented for the solution of the compressible Euler equations over unstructured grids in cylindrical and spherical coordinates. The proposed scheme is based on a mixed finite volume / finite element approach. Numerical simulations are presented for the explosion problem in two spatial dimensions in cylindrical and spherical coordinates, and the numerical results are compared with the one-dimensional simulation for cylindrically and spherically symmetric explosions.

1 INTRODUCTION

Some gasdynamics problems exhibit such strong symmetries that could be more convenient to describe these problems in a curvilinear reference, i.e. cylindrical or spherical, rather than in a Cartesian one. These are, e.g., astrophysical flows, Inertial Confinement Fusion (ICF) applications, sonoluminescence phenomena and nuclear explosions [1].

To compute the numerical solution of the compressible flow equations for these kind of flows, an interesting possibility is provided by the use of a mixed finite volume (FV) / finite element (FE) approach [2]. For example, in viscous flows, it is possible to use the FV and the FE to compute the advection and dissipation terms, respectively, within the same algorithm.

The combined use of these two different techniques is made possible by the introduction of suitable equivalence conditions that relate the FV metrics, i.e. cell volumes and inte-

grated normals, to the FE integrals. Equivalence conditions relating FV and FE schemes have been derived for Cartesian coordinates in two and three spatial dimensions [3],[4] and for cylindrical coordinates in axially symmetric two-dimensional problems [6]. In both cited references, equivalence conditions are obtained by neglecting higher order FE contributions. Subsequently in [7], equivalence conditions for the cylindrical coordinates have been derived for the first time without introducing any approximation into the FE discrete expression of the divergence operator, and in [8] the differences between the consistent scheme and an alternative one violating the the equivalence conditions have been quantified for the case of one-dimensional problems in cylindrical and spherical coordinates. In the present paper the consistent formulation is presented in the cylindrical and spherical reference systems. Numerical results for the explosion problem are also provided to demonstrate the correctness of the proposed approach.

The present paper is structured as follows. In section 2, the scalar equations in cylindrical and spherical coordinates are introduced. In sections 3 and 4 the spatial discretizations of the scalar equation by FE and FV are presented in cylindrical and spherical coordinates respectively. Equivalence conditions between FE and FV metrics are also shown. In section 3, numerical simulations are presented for the explosion problem in the cylindrical coordinates on the R–θ plane and in the the spherical coordinates on the r–ϕ plane. Numerical results are also compared to one-dimensional simulations.

2 SCALAR EQUATIONS IN CYLINDRICAL AND SPHERICAL COORDINATES

For simplicity we consider first a multidimensional scalar conservation law. The model equation in a three-dimensional cylindrical reference reads

$$\frac{\partial u}{\partial t} + \frac{\partial f_Z}{\partial Z} + \frac{1}{R}\frac{\partial}{\partial R}(R f_R) + \frac{1}{R}\frac{\partial f_\theta}{\partial \theta} = 0, \tag{1}$$

where t is the time, Z, R and θ are the axial, radial and azimuthal coordinates, respectively, $u = u(Z, R, \theta, t)$ is the scalar unknown and $\boldsymbol{f}^{\varnothing}(u) = (f_Z, f_R, f_\theta)$ is the so-called flux function. A more compact form of the above equation is obtained by introducing the divergence operator in three-dimensional cylindrical coordinates $\boldsymbol{\nabla}^{\varnothing}\boldsymbol{\cdot}\,(\cdot)$ as follows

$$\frac{\partial (u)}{\partial t} + \boldsymbol{\nabla}^{\varnothing}\boldsymbol{\cdot}\,\boldsymbol{f}^{\varnothing}(u) = 0. \tag{2}$$

The model equation in a three-dimensional spherical reference reads

$$\frac{\partial u}{\partial t} + \frac{1}{r^2}\frac{\partial}{\partial r}(r^2 f_r) + \frac{1}{r\sin\theta}\frac{\partial}{\partial \theta}(\sin\theta f_\theta) + \frac{1}{r\sin\theta}\frac{\partial f_\phi}{\partial \phi} = 0,$$

where r, θ and ϕ are the radial, polar and azimuthal coordinates, respectively, $u = u(r, \theta, \phi, t)$ is the scalar unknown and $\boldsymbol{f}^{\odot}(u) = (f_r, f_\theta, f_\phi)$ is the flux function. In a

compact form, using the divergence operator in three-dimensional spherical coordinates $\boldsymbol{\nabla}^{\odot}\boldsymbol{\cdot}\,(\cdot)$, it can be rearranged as

$$\frac{\partial(u)}{\partial t} + \boldsymbol{\nabla}^{\odot}\boldsymbol{\cdot}\,\boldsymbol{f}^{\odot}(u) = 0. \tag{3}$$

3 FINITE VOLUME/ELEMENT METHOD IN CYLINDRICAL COORDINATES

3.1 Node-pair finite element discretization

The scalar conservation law (2) is now written in a weak form by multiplying it by the radial coordinate R and by a suitable Lagrangian test function $\phi_i \in V_h \subset H^1(\Omega)$. Integrating over the support Ω_i of φ_i gives

$$\int_{\Omega_i} R\varphi_i \frac{\partial u}{\partial t}\, d\Omega_i + \int_{\Omega_i} R\varphi_i \boldsymbol{\nabla}^{\varnothing}\boldsymbol{\cdot}\,\boldsymbol{f}^{\varnothing}(u)\, d\Omega_i = 0, \quad \forall i \in \mathcal{N}, \tag{4}$$

where $\mathcal{N}$ is the set of all nodes of the triangulation. Note that by multiplying by R, the numerical singularity of the cylindrical reference system is formally removed [6]. In the following, to simplify the notation, the infinitesimal volume $d\Omega = RdRd\theta dZ$ is not indicated in the integrals. Integrating by parts immediately gives

$$\int_{\Omega_i} R\varphi_i \frac{\partial u}{\partial t} = \int_{\Omega_i} R\boldsymbol{f}^{\varnothing}\boldsymbol{\cdot}\,\boldsymbol{\nabla}^{\varnothing}\varphi_i + \int_{\Omega_i} \varphi_i \boldsymbol{f}^{\varnothing}\boldsymbol{\cdot}\,\boldsymbol{\nabla}^{\varnothing} R - \int_{\partial\Omega_i^{\partial}} R\varphi_i \boldsymbol{f}^{\varnothing}\boldsymbol{\cdot}\,\boldsymbol{n}_i^{\varnothing} \tag{5}$$

where $\partial\Omega_i^{\partial} = \partial\Omega_i \cap \partial\Omega$, with $\partial\Omega_i$ and $\partial\Omega$ are the boundary of Ω_i and of the computational domain Ω, respectively, and where $\boldsymbol{n}_i^{\varnothing} = n_Z\hat{\boldsymbol{Z}} + n_R\hat{\boldsymbol{R}} + n_\theta\hat{\boldsymbol{\theta}}$ is the outward normal versor to Ω_i. The scalar unknown is now interpolated as

$$u(Z,R,\theta,t) \simeq u_h(Z,R,\theta,t) = \sum_{k\in\mathcal{N}} u_k(t)\varphi_k(Z,R,\theta),$$

and the flux function $\boldsymbol{f}^{\varnothing}(u_h)$ is now expanded using the same shape functions $\phi_h \in V_h$ [9] as follows

$$\boldsymbol{f}^{\varnothing}\big(u_h\big) = \boldsymbol{f}^{\varnothing}\left(\sum_{k\in\mathcal{N}} u_k(t)\varphi_k(Z,R,\theta)\right) \simeq \sum_{k\in\mathcal{N}} \boldsymbol{f}_k^{\varnothing}(t)\varphi_k(Z,R,\theta),$$

to obtain

$$\sum_{k\in\mathcal{N}_i} M_{ik}^{\varnothing}\frac{\mathrm{d}u_k}{\mathrm{d}t} = \sum_{k\in\mathcal{N}_i} \boldsymbol{f}_k^{\varnothing}(t)\boldsymbol{\cdot}\int_{\Omega_{ik}} R\varphi_k\boldsymbol{\nabla}^{\varnothing}\varphi_i + \sum_{k\in\mathcal{N}_i} \boldsymbol{f}_k^{\varnothing}(t)\boldsymbol{\cdot}\int_{\Omega_{ik}} \varphi_i\varphi_k\boldsymbol{\nabla}^{\varnothing} R$$
$$- \sum_{k\in\mathcal{N}_i^{\partial}} \boldsymbol{f}_k^{\varnothing}(t)\boldsymbol{\cdot}\int_{\partial\Omega_{ik}^{\partial}} R\varphi_i\varphi_k\boldsymbol{n}_i^{\varnothing},$$

where $\mathcal{N}_i$ is the set of shape functions φ_k whose support Ω_k overlap Ω_i of φ_i, $\mathcal{N}_i^\partial$ is the set of all boundary nodes of Ω_i, $\Omega_{ik} = \Omega_i \cap \Omega_k$ and $\partial\Omega_{ik}^\partial = \partial\Omega_i \cap \partial\Omega_k \cap \partial\Omega$ The previous equation simplifies to [6]

$$\begin{aligned}\sum_{k\in N_i} M_{ik}^\varnothing \frac{\mathrm{d}u_k}{\mathrm{d}t} = -\sum_{k\in N_i,\neq}\left(\frac{\boldsymbol{f}_k^\varnothing + \boldsymbol{f}_i^\varnothing}{2}\cdot\boldsymbol{\eta}_{ik}^\varnothing - \frac{\boldsymbol{f}_k^\varnothing - \boldsymbol{f}_i^\varnothing}{2}\cdot\boldsymbol{\zeta}_{ik}^\varnothing\right)\\ + \boldsymbol{f}_i^\varnothing\cdot\widehat{\boldsymbol{L}}_i^\varnothing - \sum_{k\in\mathcal{N}_{i,\neq}^\partial}\frac{\boldsymbol{f}_k^\varnothing - \boldsymbol{f}_i^\varnothing}{2}\cdot\boldsymbol{\chi}_{ik}^\varnothing - \boldsymbol{f}_i^\varnothing\cdot\boldsymbol{\xi}_i^\varnothing,\end{aligned} \tag{6}$$

where $\mathcal{N}_{i,\neq} = \mathcal{N}_i\backslash\{i\}$ and $\mathcal{N}_{i,\neq}^\partial = \mathcal{N}_i^\partial\backslash\{i\}$, and the following FE metric quantities have been introduced

$$M_{ik}^\varnothing \overset{\text{def}}{=} \int_{\Omega_{ik}} R\varphi_i\varphi_k, \qquad M_{ik} \overset{\text{def}}{=} \int_{\Omega_{ik}} \varphi_i\varphi_k, \qquad \boldsymbol{\zeta}_{ik}^\varnothing \overset{\text{def}}{=} \int_{\Omega_{ik}} \varphi_i\varphi_k\hat{\boldsymbol{R}}, \qquad \widehat{\boldsymbol{L}}_i^\varnothing \overset{\text{def}}{=} \sum_{k\in\mathcal{N}_i}\boldsymbol{\zeta}_{ik}^\varnothing = \int_{\Omega_{ik}}\varphi_i\hat{\boldsymbol{R}},$$

$$\boldsymbol{\eta}_{ik}^\varnothing \overset{\text{def}}{=} \int_{\Omega_{ik}} R(\varphi_i\boldsymbol{\nabla}^\varnothing\varphi_k - \varphi_k\boldsymbol{\nabla}^\varnothing\varphi_i), \qquad \boldsymbol{\chi}_{ik}^\varnothing \overset{\text{def}}{=} \int_{\partial\Omega_{ik}^\partial} R\varphi_i\varphi_k, \qquad \boldsymbol{\xi}_i^\varnothing \overset{\text{def}}{=} \int_{\partial\Omega_{ik}^\partial} R\varphi_i.$$

In the next section, the corresponding FV metrics are derived.

3.2 Edge-based finite volume discretization

The spatially discrete form of the scalar conservation law (2) is now obtained according to the node-centred finite volume approach [10]. To this purpose, the integral form of (2) times the radial coordinate R is enforced over a finite number of non-overlapping finite volumes $\mathcal{C}_i$, with boundary $\partial\mathcal{C}_i$. Over each control volume $\mathcal{C}_i$ the cell-averaged unknown is introduced as follows

$$u(Z,R,\theta,t) \simeq u_i(t) = \frac{1}{V_i}\int_{\mathcal{C}_i} u(Z,R,\theta,t),$$

where V_i is the volume of the i-th cell. Splitting the boundary integral into interface and edge contributions

$$V_i^\varnothing\frac{\mathrm{d}u_i}{\mathrm{d}t} = -\sum_{k\in\mathcal{N}_{i,\neq}}\int_{\partial\mathcal{C}_{ik}} R\boldsymbol{f}^\varnothing\cdot\boldsymbol{n}_i^\varnothing - \int_{\partial\mathcal{C}_i^\partial} R\boldsymbol{f}^\varnothing\cdot\boldsymbol{n}_i^\varnothing + \int_{\mathcal{C}_i}\boldsymbol{f}^\varnothing\cdot\hat{\boldsymbol{R}}, \tag{7}$$

where $\mathcal{N}_{i,\neq}$ is the set of the finite volume $\mathcal{C}_k$ sharing a boundary with $\mathcal{C}_i$, excluding $\mathcal{C}_i$ and where $\partial\mathcal{C}_{ik} = \partial\mathcal{C}_i \cap \partial\mathcal{C}_k \neq \emptyset, k \neq i$, is the so-called cell interface. As it is standard practice, the flux vector is assumed to be constant over each cell interface. Under this assumption, the domain and boundary contributions read

$$\int_{\partial\mathcal{C}_{ik}} R\boldsymbol{f}^\varnothing\cdot\boldsymbol{n}_i^\varnothing \simeq \boldsymbol{f}_{ik}^\varnothing\cdot\int_{\partial\mathcal{C}_{ik}} R\boldsymbol{n}_i^\varnothing = \boldsymbol{f}_{ik}^\varnothing\cdot\boldsymbol{\nu}_{ik}^\varnothing \qquad \text{with} \qquad \boldsymbol{\nu}_{ik}^\varnothing \overset{\text{def}}{=} \int_{\partial\mathcal{C}_{ik}} R\boldsymbol{n}_i^\varnothing \qquad \text{and}$$

$$\int_{\partial\mathcal{C}_i^\partial} R\boldsymbol{f}^\varnothing\cdot\boldsymbol{n}_i^\varnothing \simeq \boldsymbol{f}_i^\varnothing\cdot\int_{\partial\mathcal{C}_i^\partial} R\boldsymbol{n}_i^\varnothing = \boldsymbol{f}_i^\varnothing\cdot\boldsymbol{\nu}_i^\varnothing \qquad \text{with} \qquad \boldsymbol{\nu}_i^\varnothing \overset{\text{def}}{=} \int_{\partial\mathcal{C}_i^\partial} R\boldsymbol{n}_i^\varnothing,$$

respectively. If a second-order centred approximation of the fluxes is considered, namely, $\boldsymbol{f}_{ik} = (\boldsymbol{f}_i^{\varnothing} + \boldsymbol{f}_k^{\varnothing})/2$, the final form of the finite volume approximation of (2) reads,

$$V_i^{\varnothing} \frac{\mathrm{d}u_i}{\mathrm{d}t} = - \sum_{k \in \mathcal{N}_{i,\neq}} \frac{\boldsymbol{f}_i^{\varnothing} + \boldsymbol{f}_k^{\varnothing}}{2} \cdot \boldsymbol{\nu}_{ik}^{\varnothing} + \boldsymbol{f}_i^{\varnothing} \cdot \widehat{\boldsymbol{V}}_i^{\varnothing} - \boldsymbol{f}_i^{\varnothing} \cdot \boldsymbol{\nu}_i^{\varnothing} \quad \text{with } \widehat{\boldsymbol{V}}_i^{\varnothing} \stackrel{\text{def}}{=} \int_{\mathcal{C}_i} \hat{\boldsymbol{R}}, \tag{8}$$

to be compared with the corresponding FE discretization (6).

3.3 Finite Element/Volume equivalence

The equivalence conditions relating the above FV metric quantities and the FE ones defined in the previous section are now derived. To this purpose, relevant properties of the FE and FV discretizations are briefly recalled.

Considering FE metric quantities first, from its definition the vector $\boldsymbol{\eta}_{ik}^{\varnothing}$ is asymmetric, namely, $\boldsymbol{\eta}_{ik}^{\varnothing} = -\boldsymbol{\eta}_{ki}^{\varnothing}$ which will be referred in the following as property FEM-a. Property FEM-b is obtained by noting that $\sum_{k \in \mathcal{N}_i} (\boldsymbol{\eta}_{ik}^{\varnothing} - \boldsymbol{\zeta}_{ik}^{\varnothing}) + \boldsymbol{\xi}_i^{\varnothing} = \boldsymbol{0}$ which gives immediately

$$\widehat{\boldsymbol{L}}_i^{\varnothing} = \sum_{k \in \mathcal{N}_{i,\neq}} \boldsymbol{\eta}_{ik}^{\varnothing} + \boldsymbol{\xi}_i^{\varnothing}. \tag{9}$$

Property FEM-c stems from the following identity

$$3L_i^{\varnothing} = \int_{\Omega_i} R\varphi_i \boldsymbol{\nabla}^{\varnothing} \cdot \boldsymbol{p}^{\varnothing} = \int_{\partial\Omega_i^{\partial}} R\varphi_i \boldsymbol{p}^{\varnothing} \cdot \boldsymbol{n}_i^{\varnothing} - \int_{\Omega_i} \varphi_i \boldsymbol{p}^{\varnothing} \cdot \hat{\boldsymbol{R}} - \int_{\Omega_i} R\boldsymbol{p}^{\varnothing} \cdot \boldsymbol{\nabla}^{\varnothing} \varphi_i. \tag{10}$$

By substituting the exact expansion $\boldsymbol{p}^{\varnothing} = \sum_{k \in \mathcal{N}_i} \boldsymbol{p}_k^{\varnothing} \varphi_k$, and applying node-pair representation described in section 4.1, Eq. (10) can be written as

$$\begin{aligned} 3L_i^{\varnothing} = & \sum_{k \in \mathcal{N}_{i,\neq}} \left[\frac{\boldsymbol{p}_k^{\varnothing} + \boldsymbol{p}_i^{\varnothing}}{2} \cdot \boldsymbol{\eta}_{ik}^{\varnothing} - \frac{\boldsymbol{p}_k^{\varnothing} - \boldsymbol{p}_i^{\varnothing}}{2} \cdot \boldsymbol{\zeta}_{ik}^{\varnothing} \right] \\ & - \widehat{\boldsymbol{L}}_i^{\varnothing} \cdot \boldsymbol{p}_i^{\varnothing} + \sum_{k \in \mathcal{N}_{i,\neq}^{\partial}} \frac{\boldsymbol{p}_k^{\varnothing} - \boldsymbol{p}_i^{\varnothing}}{2} \cdot \boldsymbol{\chi}_{ik}^{\varnothing} + \boldsymbol{p}_i^{\varnothing} \cdot \boldsymbol{\xi}_i^{\varnothing}. \end{aligned}$$

By substituting property FEM-b in the above identity, one finally obtain property FEM-c as

$$3L_i^{\varnothing} = \sum_{k \in \mathcal{N}_{i,\neq}} \left[\frac{\boldsymbol{p}_k^{\varnothing} + \boldsymbol{p}_i^{\varnothing}}{2} \cdot \boldsymbol{\eta}_{ik}^{\varnothing} - \frac{\boldsymbol{p}_k^{\varnothing} - \boldsymbol{p}_i^{\varnothing}}{2} \cdot \boldsymbol{\zeta}_{ik}^{\varnothing} \right] + \sum_{k \in \mathcal{N}_{i,\neq}^{\partial}} \frac{\boldsymbol{p}_k^{\varnothing} - \boldsymbol{p}_i^{\varnothing}}{2} \cdot \boldsymbol{\chi}_{ik}^{\varnothing}. \tag{11}$$

Considering now FV metric quantities, from the fact that $\boldsymbol{n}_i^{\varnothing} = -\boldsymbol{n}_k^{\varnothing}$ over $\partial\mathcal{C}_{ik}$, property FVM-a reads $\boldsymbol{\nu}_{ik}^{\varnothing} = -\boldsymbol{\nu}_{ki}^{\varnothing}$, which corresponds to the conservation property of the scheme. From the Gauss theorem, one also has

$$\int_{\mathcal{C}_i} \boldsymbol{\nabla}^{\varnothing} R = \oint_{\partial\mathcal{C}_i} R\boldsymbol{n}_i^{\varnothing},$$

which, from the definition of FV metric quantities, gives property FVM-b as

$$\widehat{\boldsymbol{V}}_i^{\varnothing} = \sum_{k \in \mathcal{N}_{i,\neq}} \boldsymbol{\nu}_{ik}^{\varnothing} + \boldsymbol{\nu}_i^{\varnothing}. \tag{12}$$

Property FVM-c is obtained by noting that

$$3V_i^{\varnothing} = \int_{\mathcal{C}_i} R \boldsymbol{\nabla}^{\varnothing} \cdot \boldsymbol{p}^{\varnothing} = \oint_{\partial \mathcal{C}_i} R \boldsymbol{p}^{\varnothing} \cdot \boldsymbol{n}_i^{\varnothing} - \int_{\mathcal{C}_i} \hat{\boldsymbol{R}} \cdot \boldsymbol{p}^{\varnothing}. \tag{13}$$

The right hand side of (13) is now computed by means of the FV discretization described in section 3.2 as

$$3V_i^{\varnothing} = \sum_{k \in \mathcal{N}_{i,\neq}} \frac{\boldsymbol{p}_k^{\varnothing} + \boldsymbol{p}_i^{\varnothing}}{2} \cdot \boldsymbol{\nu}_{ik}^{\varnothing} - \boldsymbol{p}_i^{\varnothing} \cdot \widehat{\boldsymbol{L}}_i^{\varnothing} + \boldsymbol{p}_i^{\varnothing} \cdot \boldsymbol{\nu}_i^{\varnothing}.$$

which from property FVM-b becomes

$$3V_i^{\varnothing} = \sum_{k \in \mathcal{N}_{i,\neq}} \frac{\boldsymbol{p}_k^{\varnothing} + \boldsymbol{p}_i^{\varnothing}}{2} \cdot \boldsymbol{\nu}_{ik}^{\varnothing}. \tag{14}$$

Therefore, a FV approximation can be formally obtained from FE metric quantities defined over the same grid points by setting (see properties FEM/FVM-a and -b)

$$\boldsymbol{\nu}_{ik}^{\varnothing} = \boldsymbol{\eta}_{ik}^{\varnothing}, \quad \boldsymbol{\nu}_i^{\varnothing} = \boldsymbol{\xi}_i^{\varnothing}, \quad \widehat{\boldsymbol{V}}_i^{\varnothing} = \widehat{\boldsymbol{L}}_i^{\varnothing}.$$

Note that the mass lumping approximation,

$$\sum_{k \in N_i} M_{ik}^{\varnothing} \frac{\mathrm{d}u_k}{\mathrm{d}t} \simeq L_i^{\varnothing} \frac{\mathrm{d}u_i}{\mathrm{d}t}$$

has to be introduced in the Eq. (6) for the equivalence conditions to be applicable. By subtracting Eq. (11) to Eq. (14), one finally has

$$V_i^{\varnothing} = L_i^{\varnothing} + \sum_{k \in \mathcal{N}_{i,\neq}} \frac{\boldsymbol{p}_k^{\varnothing} - \boldsymbol{p}_i^{\varnothing}}{6} \cdot \boldsymbol{\zeta}_{ik}^{\varnothing} - \sum_{k \in \mathcal{N}_{i,\neq}^{\partial}} \frac{\boldsymbol{p}_k^{\varnothing} - \boldsymbol{p}_i^{\varnothing}}{6} \cdot \boldsymbol{\chi}_{ik}^{\varnothing}. \tag{15}$$

It is remarkable that, differently from the Cartesian case [3, 4], in the cylindrical reference the FV cell is not coincident with the FE lumped mass matrix. Moreover, the shape of the FV cells that guarantees equivalence with FE discretization still remains to be determined.

4 FINITE VOLUME/ELEMENT METHOD IN SPHERICAL COORDINATES

4.1 Node-pair finite element discretization

In the present section the spatial discretization of conservation law in a spherical reference system is presented.

The scalar conservation law (3) is multiplied by the quantity $r \sin\theta$ to formally remove the singularity of the spherical coordinate system along the zenith direction. The FE node-pair discretization is obtained as done in the cylindrical case, namely

$$\begin{aligned} M_{ik}^{\odot} \frac{\mathrm{d}u_i}{\mathrm{d}t} = &- \sum_{k \in \mathcal{N}_{i,\neq}} \left(\frac{\boldsymbol{f}_k^{\odot} + \boldsymbol{f}_i^{\odot}}{2} \cdot \boldsymbol{\eta}_{ik}^{\odot} - \frac{\boldsymbol{f}_k^{\odot} - \boldsymbol{f}_i^{\odot}}{2} \cdot \boldsymbol{\zeta}_{ik}^{\odot} \right) + \boldsymbol{f}_i^{\odot} \cdot \widehat{\boldsymbol{L}}_i^{\odot} \\ &- \sum_{k \in \mathcal{N}_{i,\neq}^{\partial}} \frac{\boldsymbol{f}_k^{\odot} - \boldsymbol{f}_i^{\odot}}{2} \cdot \boldsymbol{\chi}_{ik}^{\odot} - \boldsymbol{f}_i^{\odot} \cdot \boldsymbol{\xi}_i^{\odot}, \end{aligned} \tag{16}$$

where $\mathcal{N}_{i,\neq} = \mathcal{N} \setminus \{i\}$ and $\mathcal{N}_{i,\neq}^{\partial} = \mathcal{N}^{\partial} \setminus \{i\}$ and the following metric quantities have been introduced

$$\begin{aligned} M_{ik}^{\odot} &\stackrel{\text{def}}{=} \int_{\Omega_{ik}} r \sin\theta \varphi_i \varphi_k \, d\Omega^{\odot}, & \boldsymbol{\eta}_{ik}^{\odot} &\stackrel{\text{def}}{=} \int_{\Omega_{ik}} r \sin\theta (\varphi_i \boldsymbol{\nabla}^{\odot} \varphi_k - \varphi_k \boldsymbol{\nabla}^{\odot} \varphi_i), \\ \boldsymbol{\zeta}_{ik}^{\odot} &\stackrel{\text{def}}{=} \int_{\Omega_{ik}} \varphi_i \varphi_k \hat{\boldsymbol{r}}, & \widehat{\boldsymbol{L}}_i^{\odot} &\stackrel{\text{def}}{=} \sum_{k \in \mathcal{N}_i} \boldsymbol{\zeta}_{ik}^{\odot}, \\ \boldsymbol{\chi}_{ik}^{\odot} &\stackrel{\text{def}}{=} \int_{\partial\Omega_{ik}^{\partial}} r \sin\theta \varphi_i \varphi_k, & \boldsymbol{\xi}_i^{\odot} &\stackrel{\text{def}}{=} \int_{\partial\Omega_{ik}^{\partial}} r \sin\theta \varphi_i. \end{aligned}$$

4.2 Edge-based finite volume discretization

The FV spatially discrete form of the scalar conservation law (3) multiplied by the quantity $r \sin\theta$ reads

$$V_i^{\odot} \frac{\mathrm{d}u_i}{\mathrm{d}t} = -\sum_{k \in \mathcal{N}_{i,\neq}} \frac{\boldsymbol{f}_i^{\odot} + \boldsymbol{f}_k^{\odot}}{2} \cdot \boldsymbol{\nu}_{ik}^{\odot} + \boldsymbol{f}_i^{\odot} \cdot \widehat{\boldsymbol{V}}_i^{\odot} - \boldsymbol{f}_i^{\odot} \cdot \boldsymbol{\nu}_i^{\odot} \tag{17}$$

where

$$\widehat{\boldsymbol{V}}_i^{\odot} \stackrel{\text{def}}{=} \int_{\partial \mathcal{C}_i^{\partial}} \hat{\boldsymbol{r}}, \quad \boldsymbol{\nu}_{ik}^{\odot} \stackrel{\text{def}}{=} \int_{\partial \mathcal{C}_{ik}} r \sin\theta \boldsymbol{n}_i^{\odot} \quad \text{and} \quad \boldsymbol{\nu}_i^{\odot} \stackrel{\text{def}}{=} \int_{\partial \mathcal{C}_i^{\partial}} r \sin\theta \boldsymbol{n}_i^{\odot}$$

4.3 Finite Element/Volume equivalence

The equivalence conditions relating the FV and FE scheme are obtained like in the cylindrical case. The following properties are introduced for the FE metric quantities

$$\begin{aligned} \boldsymbol{\eta}_{ik}^{\odot} &= -\boldsymbol{\eta}_{ki}^{\odot} \quad (\mathrm{FEM-a}), \qquad \widehat{\boldsymbol{L}}_i^{\odot} = \sum_{k \in \mathcal{N}_{i,\neq}} \boldsymbol{\eta}_{ik}^{\odot} + \boldsymbol{\xi}_i^{\odot} \quad (\mathrm{FEM-b}), \\ 3L_i^{\odot} &= \int_{\partial\Omega_i^{\partial}} r \sin\theta \varphi_i \boldsymbol{x}^{\odot} \cdot \boldsymbol{n}_i^{\odot} - \int_{\Omega_i} \varphi_i \boldsymbol{x}^{\odot} \cdot \hat{\boldsymbol{r}} - \int_{\Omega_i} r \sin\theta \boldsymbol{x}^{\odot} \cdot \boldsymbol{\nabla}^{\odot} \varphi_i, \quad (\mathrm{FEM-c}) \end{aligned} \tag{18}$$

and for the FV metric quantities

$$\begin{aligned} \boldsymbol{n}_i^{\odot} &= -\boldsymbol{n}_k^{\odot} \quad (\mathrm{FVM-a}), \qquad \widehat{\boldsymbol{V}}_i^{\odot} = \sum_{k \in \mathcal{N}_{i,\neq}} \boldsymbol{\nu}_{ik}^{\odot} + \boldsymbol{\nu}_i^{\odot} \quad (\mathrm{FVM-b}), \\ 3V_i^{\odot} &= \sum_{k \in \mathcal{N}_{i,\neq}} \frac{\boldsymbol{x}_i^{\odot} + \boldsymbol{x}_k^{\odot}}{2} \cdot \boldsymbol{\nu}_{ik}^{\odot}. \quad (\mathrm{FVM-c}) \end{aligned} \tag{19}$$

Therefore, a FV approximation can be formally obtained from FE metric quantities defined over the same grid points by setting (see properties FEM/FVM-a and -b)

$$\boldsymbol{\nu}_{ik}^{\odot} = \boldsymbol{\eta}_{ik}^{\odot}, \quad \boldsymbol{\nu}_i^{\odot} = \boldsymbol{\xi}_i^{\odot}, \quad \widehat{\boldsymbol{V}}_i^{\odot} = \widehat{\boldsymbol{L}}_i^{\odot}.$$

By subtracting (FEM–c) to (FVM–c), one finally has

$$V_i^{\odot} = L_i^{\odot} + \sum_{k \in \mathcal{N}_{i,\neq}} \frac{\boldsymbol{x}_k^{\odot} - \boldsymbol{x}_i^{\odot}}{6} \cdot \boldsymbol{\zeta}_{ik}^{\odot} - \sum_{k \in \mathcal{N}_{i,\neq}^{\partial}} \frac{\boldsymbol{x}_k^{\odot} - \boldsymbol{x}_i^{\odot}}{6} \cdot \boldsymbol{\chi}_{ik}^{\odot}, \tag{20}$$

where, like the cylindrical case, the mass lumping approximation has been introduced. It is clear that also in this case he FV cell is not coincident with the FE lumped mass matrix and the shape of the FV cells that guarantees equivalence with FE discretization still remains undetermined.

5 FULLY DISCRETE FORM OF THE EULER EQUATIONS IN CYLINDRICAL AND SPHERICAL COORDINATES

The Euler equations in cylindrical and spherical coordinates for compressible inviscid flows are now briefly recalled. The differential form reads

$$\frac{\partial \mathbf{u}^{\varnothing}}{\partial t} + \boldsymbol{\nabla}^{\varnothing} \cdot \mathbf{f}^{\varnothing} = \frac{1}{R} \boldsymbol{s}^{\varnothing} \quad \text{and} \quad \frac{\partial \mathbf{u}^{\odot}}{\partial t} + \boldsymbol{\nabla}^{\odot} \cdot \mathbf{f}^{\odot} = \frac{1}{r \sin\theta} \boldsymbol{s}^{\odot},$$

where $\mathbf{u}^{\varnothing}(Z, R, \theta, t) = (\rho, \boldsymbol{m}^{\varnothing}, E^{\mathrm{t}})^{\mathrm{T}}$ and $\mathbf{u}^{\odot}(r, \theta, \phi, t) = (\rho, \boldsymbol{m}^{\odot}, E^{t})^{\mathrm{T}}$, with ρ density, $\boldsymbol{m}^{\varnothing} = (m_Z, m_R, m_\theta)^{\mathrm{T}}$, $\boldsymbol{m}^{\odot} = (m_r, m_\theta, m_\phi)^{\mathrm{T}}$ momentum and E^t total energy per unit

volume. The flux function and the source term are defined as follow in the cylindrical case

$$\mathbf{f}^{\varnothing} = \begin{pmatrix} m_Z & m_R & m_\theta \\ \frac{m_Z^2}{\rho} + \Pi & \frac{m_R m_Z}{\rho} & \frac{m_\theta m_Z}{\rho} \\ \frac{m_Z m_R}{\rho} & \frac{m_R^2}{\rho} + \Pi & \frac{m_\theta m_R}{\rho} \\ \frac{m_Z m_\theta}{\rho} & \frac{m_R m_\theta}{\rho} & \frac{m_\theta^2}{\rho} + \Pi \\ \frac{m_Z}{\rho}\left(E^t + \Pi\right) & \frac{m_R}{\rho}\left(E^t + \Pi\right) & \frac{m_\theta}{\rho}\left(E^t + \Pi\right) \end{pmatrix}, \quad \boldsymbol{s}^{\varnothing} = \begin{pmatrix} 0 \\ 0 \\ \frac{m_\theta^2}{\rho} + \Pi \\ \frac{m_\theta m_R}{\rho} \\ 0 \end{pmatrix},$$

and in the spherical one

$$\mathbf{f}^{\odot}(\mathbf{u}^{\odot}) = \begin{pmatrix} m_r & m_\theta & m_\phi \\ \frac{m_r^2}{\rho} + \Pi & \frac{m_\theta m_r}{\rho} & \frac{m_\phi m_r}{\rho} \\ \frac{m_r m_\theta}{\rho} & \frac{m_\theta^2}{\rho} + \Pi & \frac{m_\phi m_\theta}{\rho} \\ \frac{m_r m_\phi}{\rho} & \frac{m_\theta m_\phi}{\rho} & \frac{m_\phi^2}{\rho} + \Pi \\ \frac{m_r}{\rho}\left(E^t + \Pi\right) & \frac{m_\theta}{\rho}\left(E^t + \Pi\right) & \frac{m_\phi}{\rho}\left(E^t + \Pi\right) \end{pmatrix},$$

$$\boldsymbol{s}^{\odot}(\mathbf{u}^{\odot}) = \underbrace{\begin{pmatrix} 0 \\ \left(\frac{m_\theta^2}{\rho} + \Pi\right) + \left(\frac{m_\phi^2}{\rho} + \Pi\right) \\ -\frac{m_\theta m_r}{\rho} \\ -\frac{m_\phi m_r}{\rho} \\ 0 \end{pmatrix}}_{\breve{\boldsymbol{s}}^{\odot}} \sin\theta + \underbrace{\begin{pmatrix} 0 \\ 0 \\ \frac{m_\phi^2}{\rho} + \Pi \\ -\frac{m_\phi m_\theta}{\rho} \\ 0 \end{pmatrix}}_{\bar{\boldsymbol{s}}^{\odot}} \cos\theta.$$

The FV spatially-discrete form of the Euler equations reads

$$\begin{aligned} V_i^{\varnothing} \frac{\mathrm{d}\mathbf{u}_i^{\varnothing}}{\mathrm{d}t} &= -\sum_{k \in \mathcal{N}_i, \neq} \frac{\mathbf{f}_k^{\varnothing} + \mathbf{f}_i^{\varnothing}}{2} \cdot \boldsymbol{\eta}_{ik}^{\varnothing} + L_i \boldsymbol{s}_i^{\varnothing} - \mathbf{f}_i^{\varnothing} \cdot \boldsymbol{\xi}_i^{\varnothing}, \\ V_i^{\odot} \frac{\mathrm{d}\mathbf{u}_i^{\odot}}{\mathrm{d}t} &= -\sum_{k \in \mathcal{N}_i, \neq} \frac{\mathbf{f}_i^{\odot} + \mathbf{f}_k^{\odot}}{2} \cdot \boldsymbol{\eta}_{ik}^{\odot} + \boldsymbol{f}_i^{\odot} \cdot \widehat{\boldsymbol{L}}_i^{\odot} - \boldsymbol{f}_i^{\odot} \cdot \boldsymbol{\xi}_i^{\odot} + \breve{\boldsymbol{s}}_i^{\odot} \hat{L}_i + \bar{\boldsymbol{s}}_i^{\odot} \check{L}_i, \end{aligned} \tag{21}$$

where the following notation has been used $\boldsymbol{s}_i^{\varnothing} \stackrel{\text{def}}{=} \boldsymbol{s}^{\varnothing}(\mathbf{u}_i^{\varnothing})$, $\breve{\boldsymbol{s}}_i^{\odot} \stackrel{\text{def}}{=} \breve{\boldsymbol{s}}^{\odot}(\mathbf{u}_i^{\odot})$, $\bar{\boldsymbol{s}}_i^{\odot} \stackrel{\text{def}}{=} \bar{\boldsymbol{s}}^{\odot}(\mathbf{u}_i^{\odot})$. The terms $V_i^{\varnothing}$ and $V_i^{\odot}$ are computed from the equivalence condition in cylindrical and

spherical case, respectively. In the computation, a TVD [11] numerical flux is used, with the van Leer limiter [12]. The fully discrete form of the Euler system is obtained by a two-step Backward Differencing Formulæ. At each time level, a dual time-stepping technique is used to solve the time-implicit problem [13].

6 NUMERICAL RESULTS

In the present section, numerical results for diverging cylindrical and spherical shock waves are presented in the two-dimensional cases (R–θ and r–ϕ planes) and the one-dimensional case.

Initial conditions are as follows. The velocity is assumed to be zero everywhere; the density is uniform and equal to 1, whereas the pressure is uniform and equal to 10 in a circular region centered at the origin with radius $r = 0.5$. In the remaining portion of the domain, the pressure is uniform and equal to 1. In all computations, the ideal gas model for nitrogen ($\gamma = c_P/c_v = 1.39$) is used. The thermodynamics variables are made dimensionless by the corresponding value at rest (outer region), the spatial dimensions are made dimensionless by the radius of the domain. Velocity and time are made dimensionless by the square root of the reference pressure divided by the reference density; the reference time is the reference length divided by the reference velocity.

Numerical results are shown in figure 1, for the cylindrical and for the spherical cases, where the density isolines at different time levels are shown together with the pressure profiles along the axis $y = 0$. A shock wave propagates towards the outer boundary of the computational domain; the shock wave is followed by a contact discontinuity. A rarefaction wave propagates towards the origin and is then reflected outward. The grid is the made with 39 153 nodes 77 587 triangles and the time step is 1.5×10^{-4}. The pressure profiles are compared against reference one-dimensional results for the three different time levels. One-dimensional computations were performed over a evenly-spaced grid made of 2 001 nodes, which corresponds to an element spacing of 5×10^{-4}.

7 CONCLUSIONS

A novel unstructured-grid hybrid finite element/volume method for a orthogonal curvilinear coordinates was presented. The method moves from suitable equivalence conditions linking finite element integrals to the corresponding finite volume metrics, such as the cell volume or the integrated normals. The equivalence conditions were derived here without introducing any approximation and allow to determine all needed finite volume metric quantities from finite element ones. Numerical results are presented for two-dimensional compressible flows: these consist in the numerical simulation of the explosion problem, in which an initial discontinuity in pressure results in the formation of a diverging shock. The computed pressure and density profile agree fairly well with one-dimensional simulation in cylindrical and spherical symmetry over a very fine grid.

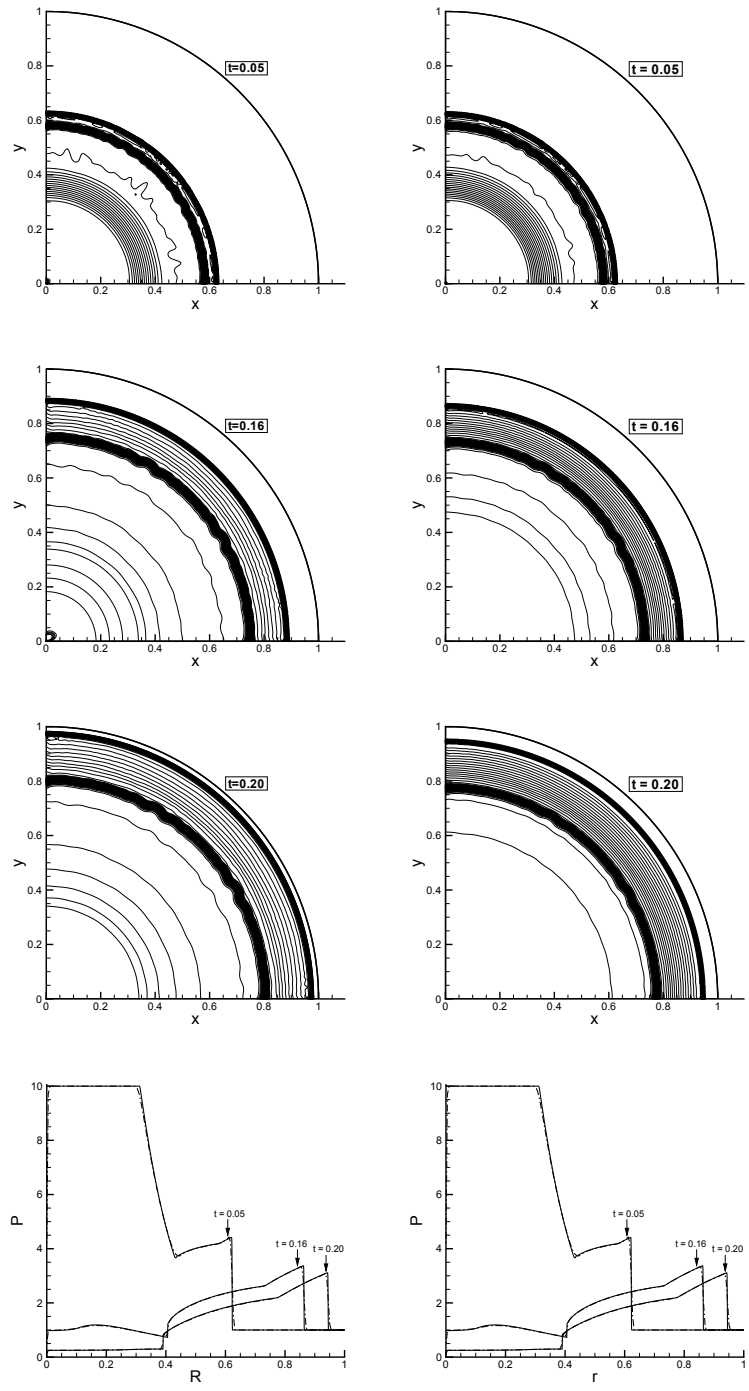

Figure 1: Density isolines for the explosion problem: left R–θ and right r–ϕ plane (Each isoline corresponds to a density difference of $\Delta\rho/\rho_{ref} = 0.03$). The pressure signal is along the axis $y = 0$. The solid line is the 1D reference solution, the dash-dotted line is the 2D solution.

REFERENCES

[1] L. I. Sedov., *Similarity and dimensional methods in mechanics.*, Academic Press, 1959.

[2] L. Fezou and B. Stoufflet., *A class of implicit upwind schemes for Euler simulations with unstructured meshes.*, J. Comput. Phys., 84(1):174–206, 1989.

[3] V. Selmin., *The node-centred finite volume approach: bridge between finite differences and finite elements.*, Comp. Meth. Appl. Mech. Engng., 102:107–138, 1993.

[4] V. Selmin. and L. Formaggia., *Unified construction of finite element and finite volume discretizations for compressible flows.*, Int. J. Numer. Meth. Eng., 39:1–32, 1996.

[5] H. B. Chen, L. Zhang, and E. Panarella., *Stability of imploding spherical shock waves.*, Journal of Fusion Energy, 14:389–392, 1995.

[6] A. Guardone and L. Vigevano., *Finite element/volume solution to axisymmetric conservation laws.*, J. Comput. Phys., 224:489–518, 2007.

[7] D. De Santis, G. Geraci, and A. Guardone, *Equivalence conditions for finite volume/ element discretizations in cylindrical coordinates.*, V European Conference on Computational Fluid Dynamics ECCOMAS CFD 2010, June 2010.

[8] A. Guardone, D. De Santis, G. Geraci, M. Pasta, *On the relation between finite element and finite volume schemes for compressible flows with cylindrical and spherical symmetry.*, J. Comput. Phys., 230:680–694, 2011.

[9] J. Donea and A. Huerta., *Finite element methods for flow problems.*, Wiley, 2002.

[10] R. J. LeVeque., *Finite volume methods for conservation laws and hyperbolic systems.*, Cambridge University Press, 2002.

[11] A. Harten and J. M. Hyman., *Self adjusting grid methods for one-dimensional hyperbolic conservation laws.*, J. Comput. Phys., 50:253–269, 1983.

[12] B. van Leer., *Towards the ultimate conservative difference scheme II. Monotoniticy and conservation combined in a second order scheme.*, J. Comput. Phys., 14:361–370,1974

[13] V. Venkatakrishnan and D. J. Mavriplis., *Implicit method for the computation of unsteady flows on unstructured grids.*, J. Comput. Phys., 127:380–397, 1996.